



Investigation of Weight Effects on the Critical Speed of Inclined Turbocharger Rotor System

Xu Ouyang¹ · Hulun Guo¹ · Xintao Wu² · Rixiu Men² · Menghan Li¹ · Shuqian Cao¹

Received: 13 February 2022 / Accepted: 25 February 2022 / Published online: 12 March 2022
© The Author(s) 2022

Abstract

Turbochargers have been widely used in various base conditions, such as horizontal, vertical, or inclined. The prediction of the dynamics is of utmost importance to inclined turbocharger designers. In this paper, the effect of weight on the critical speed of an inclined turbocharger rotor coupled with floating ring bearings is investigated. The inclined turbocharger rotor is modeled by lumped mass model. The nonlinear floating ring bearing model is derived using Capone's model. Then the nonlinear dynamic model of the turbocharger rotor system is obtained. The balance position of the turbocharger rotor system is obtained by solving the nonlinear static equation. Linear system of the turbocharger rotor system is derived based on the balance position, and the critical speed is obtained by solving an eigenvalue problem. Three vibration modes, i.e. conical whirl, cylindrical whirl, and bending are obtained. Increasing the inclined angle would decrease the critical speed. Increasing the inclined angle would decrease the critical speed. Among the three vibration modes, the critical speed of cylindrical whirl furnishes the highest decrease while the critical speed of bending attains the lowest decrease. The vertical turbocharger rotor has a more wide operating speed range than the horizontal turbocharger rotor.

Keywords Turbochargers · Floating ring bearings · Inclined rotor · Critical speed

✉ Hulun Guo
hlguo@tju.edu.cn

¹ Tianjin Key Laboratory of Nonlinear Dynamics and Control, Department of Mechanics, Tianjin University, Tianjin 300072, China

² National Key Laboratory of Diesel Engines Turbocharging Technology, China North Engine Research Institute, Tianjin 300400, China

1 Introduction

Turbochargers are a special class of turbomachinery used to increase engine power by providing compressed air for combustion. In order to meet the demand for high power production, the operating speed of turbochargers has been increased to an extremely high range. Under such circumstances, the dynamics of the turbocharger rotor system accordingly becomes inevitably challenging in the stages of product design and fault diagnosis.

Rotor dynamics of turbochargers have been studied widely. Pettinato and DeChoudhury [1] analytically and experimentally studied the critical speed and failure mechanisms for redesign a high-speed turbocharger. Chen [2] discussed the critical speed of larger turbochargers with various bearing designs. Ying et al. [3] investigated the effect of foundation excitation on the dynamical behavior of a turbocharger.

Traditionally, the turbocharger rotor-bearing unit includes two fluid lubricated floating ring bearings as well as a single overhung rotor with the compressor and turbine disks at the two ends. Measurements and simulations show that rotors supported in full-floating ring bearings exhibit diverse nonlinear oscillation effects [4–6], which originate in the high nonlinearities introduced by the floating ring bearings. Nonlinear rotor dynamics have been studied widely by different methods [7–9]. Krik et al. [10] studied the linear stability threshold speeds and the nonlinear transient response of the automotive turbocharger with varying bearing designs and properties. Schilder et al. [11] investigated the quasi-periodic oscillations of a finite beam-element turbocharger model with nonlinear oil-film forces. Schweizer [12, 13] examined the oil whirl, oil whip, whirl/whip synchronization, and the total instability of turbocharger rotors supported in full-floating ring bearings. Bonello [14] analyzed the nonlinear dynamic behavior of a turbocharger on floating ring bearings by transient modal analysis. Tian et al. [15, 16] investigated the dynamic response and synchronous and sub-synchronous vibrations of turbocharger rotor systems supported on floating ring bearings. Koutsovasilis et al. [17] applied a methodology to quantify the sub-synchronous vibrations of a turbocharger with full-floating ring bearings. Liang et al. [18] developed a method to control the magnitude and frequency of nonlinear whirl motion of turbocharger rotor using the outer clearance of semi-floating ring bearing. Smolik et al. [19] studied the effects of radial bearing clearances on the amplitudes of the sub-synchronous response of the turbocharger rotor. Zhang et al. [20] studied the impact of the reduced load capacities and bearing torques caused by circumferential or/and axial grooves in full-floating-ring bearings on the nonlinear oscillations of turbocharger rotors. Singh and Gupta [21] studied the effect of rotating unbalance and engine excitations on the nonlinear dynamic response of turbocharger flexible rotor system supported on floating ring bearings.

Turbochargers have been widely used in various base conditions, such as horizontal, vertical, or inclined. The vertical and inclined rotors have been studied by several scholars. Shi et al. [22] comprehensively studied the nonlinear dynamics of a vertical rotor-bearing system based on the bifurcation diagrams,

waterfall diagrams, rotor center orbits, Poincare maps, and frequency spectrums. Luneno et al. [23] gave a good agreement between the simulation and experimental results of a vertical rotor bearings system. Cha and Glavatskih [24] investigated the nonlinear dynamic behavior of vertical and horizontal rotors in compliant liner tilting pad journal bearings. Nishimura et al. [25] demonstrated the nonlinear steady-state vibration of the self-excited vibration of a vertical rotating shaft with journal bearing. Shi et al. [26] studied the influence of pivot design on nonlinear dynamic characteristics of a vertical and horizontal rotor. Liu et al. [27, 28] applied numerical and experimental methods to study the periodic solution and stability of the inclined rotor journal bearing system. Capone's short bearing model was employed to describe the journal bearing support properties. Xu et al. [29] investigated the vibration characteristics of an eccentric rotor with both the axially inclined angle and the orientation angle. So far, no previous work has been done on the critical speed of inclined turbocharger rotor coupled with nonlinear floating ring bearings.

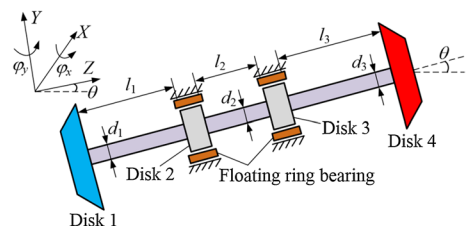
Hence, the purpose of this work is to investigate the effect of weight on the critical speed of an inclined turbocharger rotor coupled with two nonlinear floating ring bearings. Based on the lumped mass model and Capone's model, the inclined turbocharger rotor is modeled as a nonlinear dynamic system. The linear system of the turbocharger rotor system is derived using Taylor's series expansion. Then the critical speed is obtained by solving an eigenvalue problem. The influence of inclined angle on the critical speed of an inclined turbocharger rotor system is investigated in detail.

2 Dynamic Model of an Inclined Turbocharger Rotor System

2.1 Turbocharger Rotor Modeling

The structure of an inclined turbocharger rotor system is depicted in Fig. 1, where the left end is a compressor wheel, and the right end is a turbine wheel. The inclined angle θ is defined as the intersection angle of the rotor axis line and horizontal plane. When $\theta=0$, the turbocharger rotor is horizontal. When $\theta=90^\circ$, the turbocharger rotor is vertical. The shaft is supported by two floating ring bearings. The inclined turbocharger rotor is simplified to four mass nodes connected by three massless beam sections. Meanwhile, the moment of inertia of the beam elements was also concentrated on the corresponding mass nodes. m_i is the mass of the i th disk, d_i and

Fig. 1 The turbocharger rotor-bearing model



l_i are the diameter and the length of the i th shaft section, respectively. The X and Y directions are set in the disc plane, and Z direction is along with the shaft axis.

Following the way described in Ref. [3], the governing equations of motion for turbocharger rotor system are formulated as

$$m_1 \ddot{X}_1 + \frac{12EI_1}{l_1^3} X_1 + \frac{6EI_1}{l_1^2} \varphi_{y1} - \frac{12EI_1}{l_1^3} X_2 + \frac{6EI_1}{l_1^2} \varphi_{y2} = m_1 e_1 \omega^2 \cos \omega t \quad (1)$$

$$J_{a1} \ddot{\varphi}_{y1} - \omega J_{p1} \dot{\varphi}_{x1} + \frac{6EI_1}{l_1^2} X_1 + \frac{4EI_1}{l_1} \varphi_{y1} - \frac{6EI_1}{l_1^2} X_2 + \frac{2EI_1}{l_1} \varphi_{y2} = 0 \quad (2)$$

$$\begin{aligned} m_2 \ddot{X}_2 - \frac{12EI_1}{l_1^3} X_1 - \frac{6EI_1}{l_1^2} \varphi_{y1} + \left(\frac{12EI_1}{l_1^3} + \frac{12EI_2}{l_2^3} \right) X_2 + \left(-\frac{6EI_1}{l_1^2} + \frac{6EI_2}{l_2^2} \right) \varphi_{y2} \\ - \frac{12EI_2}{l_2^3} X_3 + \frac{6EI_2}{l_2^2} \varphi_{y3} = -F_{x,2}^{in} \end{aligned} \quad (3)$$

$$\begin{aligned} J_{a2} \ddot{\varphi}_{y2} - \omega J_{p2} \dot{\varphi}_{x2} + \frac{6EI_1}{l_1^2} X_1 + \frac{2EI_1}{l_1} \varphi_{y1} + \left(-\frac{6EI_1}{l_1^2} + \frac{6EI_2}{l_2^2} \right) X_2 + \left(\frac{4EI_1}{l_1} + \frac{4EI_2}{l_2} \right) \varphi_{y2} \\ - \frac{6EI_2}{l_2^2} X_3 + \frac{2EI_2}{l_2} \varphi_{y3} = 0 \end{aligned} \quad (4)$$

$$\begin{aligned} m_3 \ddot{X}_3 - \frac{12EI_2}{l_2^3} X_2 - \frac{6EI_2}{l_2^2} \varphi_{y2} + \left(\frac{12EI_2}{l_2^3} + \frac{12EI_3}{l_3^3} \right) X_3 + \left(-\frac{6EI_2}{l_2^2} + \frac{6EI_3}{l_3^2} \right) \varphi_{y3} \\ - \frac{12EI_3}{l_3^3} X_4 + \frac{6EI_3}{l_3^2} \varphi_{y4} = -F_{x,3}^{in} \end{aligned} \quad (5)$$

$$\begin{aligned} J_{a3} \ddot{\varphi}_{y3} - \omega J_{p3} \dot{\varphi}_{x3} + \frac{6EI_2}{l_2^2} X_2 + \frac{2EI_2}{l_2} \varphi_{y2} + \left(-\frac{6EI_2}{l_2^2} + \frac{6EI_3}{l_3^2} \right) X_3 + \left(\frac{4EI_2}{l_2} + \frac{4EI_3}{l_3} \right) \varphi_{y3} \\ - \frac{6EI_3}{l_3^2} X_4 + \frac{2EI_3}{l_3} \varphi_{y4} = 0 \end{aligned} \quad (6)$$

$$m_4 \ddot{X}_4 - \frac{12EI_3}{l_3^3} X_3 - \frac{6EI_3}{l_3^2} \varphi_{y3} + \frac{12EI_3}{l_3^3} X_4 - \frac{6EI_3}{l_3^2} \varphi_{y4} = m_4 e_4 \omega^2 \cos \omega t \quad (7)$$

$$J_{a4} \ddot{\varphi}_{y4} - \omega J_{p4} \dot{\varphi}_{x4} + \frac{6EI_3}{l_3^2} X_3 + \frac{2EI_3}{l_3} \varphi_{y3} - \frac{6EI_3}{l_3^2} X_4 + \frac{4EI_3}{l_3} \varphi_{y4} = 0 \quad (8)$$

$$m_1 \ddot{Y}_1 + \frac{12EI_1}{l_1^3} Y_1 - \frac{6EI_1}{l_1^2} \varphi_{x1} - \frac{12EI_1}{l_1^3} Y_2 - \frac{6EI_1}{l_1^2} \varphi_{x2} = m_1 e_1 \omega^2 \sin \omega t - m_1 g \cos \theta \tag{9}$$

$$J_{a1} \ddot{\varphi}_{x1} + \omega J_{p1} \dot{\varphi}_{y1} - \frac{6EI_1}{l_1^2} Y_1 + \frac{4EI_1}{l_1} \varphi_{x1} + \frac{6EI_1}{l_1^2} Y_2 + \frac{2EI_1}{l_1} \varphi_{x2} = 0 \tag{10}$$

$$m_2 \ddot{Y}_2 - \frac{12EI_1}{l_1^3} Y_1 + \frac{6EI_1}{l_1^2} \varphi_{x1} + \left(\frac{12EI_1}{l_1^3} + \frac{12EI_2}{l_2^3} \right) Y_2 + \left(\frac{6EI_1}{l_1^2} - \frac{6EI_2}{l_2^2} \right) \varphi_{x2} - \frac{12EI_2}{l_2^3} Y_3 - \frac{6EI_2}{l_2^2} \varphi_{y3} = -m_2 g \cos \theta - F_{y,2}^{in} \tag{11}$$

$$J_{a2} \ddot{\varphi}_{x2} + \omega J_{p2} \dot{\varphi}_{y2} - \frac{6EI_1}{l_1^2} Y_1 + \frac{2EI_1}{l_1} \varphi_{x1} + \left(\frac{6EI_1}{l_1^2} - \frac{6EI_2}{l_2^2} \right) Y_2 + \left(\frac{4EI_1}{l_1} + \frac{4EI_2}{l_2} \right) \varphi_{x2} + \frac{6EI_2}{l_2^2} Y_3 + \frac{2EI_2}{l_2} \varphi_{x3} = 0 \tag{12}$$

$$m_3 \ddot{Y}_3 - \frac{12EI_2}{l_2^3} Y_2 + \frac{6EI_2}{l_2^2} \varphi_{x2} + \left(\frac{12EI_2}{l_2^3} + \frac{12EI_3}{l_3^3} \right) Y_3 + \left(\frac{6EI_2}{l_2^2} - \frac{6EI_3}{l_3^2} \right) \varphi_{x3} - \frac{12EI_3}{l_3^3} Y_4 - \frac{6EI_3}{l_3^2} \varphi_{x4} = -m_3 g \cos \theta - F_{y,3}^{in} \tag{13}$$

$$J_{a3} \ddot{\varphi}_{x3} + \omega J_{p3} \dot{\varphi}_{y3} - \frac{6EI_2}{l_2^2} Y_2 + \frac{2EI_2}{l_2} \varphi_{y2} + \left(\frac{6EI_2}{l_2^2} - \frac{6EI_3}{l_3^2} \right) Y_3 + \left(\frac{4EI_2}{l_2} + \frac{4EI_3}{l_3} \right) \varphi_{x3} + \frac{6EI_3}{l_3^2} Y_4 + \frac{2EI_3}{l_3} \varphi_{x4} = 0 \tag{14}$$

$$m_4 \ddot{Y}_4 - \frac{12EI_3}{l_3^3} Y_3 + \frac{6EI_3}{l_3^2} \varphi_{x3} + \frac{12EI_3}{l_3^3} Y_4 + \frac{6EI_3}{l_3^2} \varphi_{x4} = m_4 e_4 \omega^2 \sin \omega t - m_4 g \cos \theta \tag{15}$$

$$J_{a4} \ddot{\varphi}_{x4} + \omega J_{p4} \dot{\varphi}_{y4} - \frac{6EI_3}{l_3^2} Y_3 + \frac{2EI_3}{l_3} \varphi_{x3} + \frac{6EI_3}{l_3^2} Y_4 + \frac{4EI_3}{l_3} \varphi_{x4} = 0 \tag{16}$$

where X_i is the displacement of the i th disk along the X axis, Y_i is the displacement of the i th disk along the Y axis, φ_{xi} is the angular displacement of the i th disk around the X axis, φ_{yi} is the angular displacement of the i th disk around the Y axis, J_{ai} is the transverse moment of inertia of the i th disk, J_{pi} is the polar moment of inertia of the i th disk, e_i is the eccentricity of the i th disk, I_i is the moment of inertia of the i th shaft, $F_{x,2}^{in}$ and $F_{x,3}^{in}$ are the inner oil film force along the X axis under the second and

third mass nodes, $F_{y,2}^{in}$ and $F_{y,3}^{in}$ are the inner oil film force along the Y axis under the second and third mass nodes, E is the modulus of elasticity of the shaft, ω is the rotational speed of the turbocharger rotor, g is the acceleration of gravity and t is time.

2.2 Floating Ring Bearing Modeling

There are two fluid films (i.e. inner and outer) in a floating ring bearing, as shown in Fig. 2. The inner fluid film is formed between the journal and the floating ring, whereas the outer film is between the floating ring and bearing housing. The fixed right-hand frame of reference coordinates O_bXY is given where O_b denotes the bearing origin. The nonlinear floating ring bearings model developed in this paper is derived in dimensional form using Capone’s model [15, 16]. The Reynolds equations for the inner and outer oil films can be written as follows:

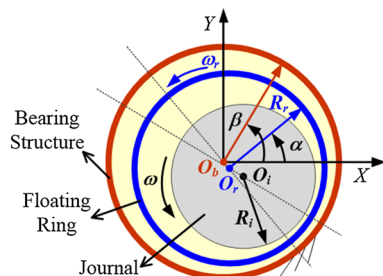
$$\begin{aligned} \frac{1}{R_i^2} \frac{\partial}{\partial \alpha} \left(\frac{h_{in}^3}{12\mu_{in}} \frac{\partial p_{in}}{\partial \alpha} \right) + \frac{\partial}{\partial Z_{in}} \left(\frac{h_{in}^3}{12\mu_{in}} \frac{\partial p_{in}}{\partial Z_{in}} \right) &= \frac{\omega + \omega_r}{2} \frac{\partial h_{in}}{\partial \alpha} + \frac{\partial h_{in}}{\partial t} \\ \frac{1}{R_r^2} \frac{\partial}{\partial \beta} \left(\frac{h_{out}^3}{12\mu_{out}} \frac{\partial p_{out}}{\partial \beta} \right) + \frac{\partial}{\partial Z_{out}} \left(\frac{h_{out}^3}{12\mu_{out}} \frac{\partial p_{out}}{\partial Z_{out}} \right) &= \frac{\omega_r}{2} \frac{\partial h_{out}}{\partial \beta} + \frac{\partial h_{out}}{\partial t} \end{aligned} \tag{17}$$

where the subscripts *in* and *out* identify the parameters of the inner oil film and outer oil film, respectively. R_i and R_r correspond to the journal radius and floating ring outer radius, respectively. α and β are the circumferential position of the inner and outer oil films, respectively. p is the oil film pressure, h is the oil film thicknesses, Z is the oil film thicknesses and μ denotes the lubricating oil viscosity, and ω_r is the rotational speed of the floating ring.

According to Fig. 2, we have

$$\begin{aligned} h_{in}(\alpha, t) &= C_{in} - x_i \cos \alpha - y_i \sin \alpha \\ h_{out}(\beta, t) &= C_{out} - X_r \cos \beta - Y_r \sin \beta \end{aligned} \tag{18}$$

Fig. 2 Floating ring bearing middle plane and reference frame



$$\begin{aligned} \frac{\partial h_{in}}{\partial t} &= -\dot{x}_i \cos \alpha - \dot{y}_i \sin \alpha \\ \frac{\partial h_{out}}{\partial t} &= -\dot{X}_r \cos \beta - \dot{Y}_r \sin \beta \end{aligned} \tag{19}$$

$$\begin{aligned} x_i &= X_i - X_r \\ y_i &= Y_i - Y_r \end{aligned} \tag{20}$$

where C_{in} and C_{out} are the radial average clearance of inner and outer oil films, (X_i, Y_i) is the displacement of journal center O_i of the i th disk, (X_r, Y_r) is the displacement of floating ring center O_r , (x_i, y_i) is the displacement of journal center O_i relative to floating ring center O_r .

Applying infinite short bearing approximation theory, Eq. (17) can be rewritten.

$$\begin{aligned} \frac{\partial}{\partial Z_{in}} \left(\frac{h_{in}^3}{12\mu_{in}} \frac{\partial p_{in}}{\partial Z_{in}} \right) &= \frac{\omega + \omega_r}{2} \frac{\partial h_{in}}{\partial \alpha} + \frac{\partial h_{in}}{\partial t} \\ \frac{\partial}{\partial Z_{out}} \left(\frac{h_{out}^3}{12\mu_{out}} \frac{\partial p_{out}}{\partial Z_{out}} \right) &= \frac{\omega_r}{2} \frac{\partial h_{out}}{\partial \beta} + \frac{\partial h_{out}}{\partial t} \end{aligned} \tag{21}$$

Substituting Eqs. (18)–(20) into Eq. (21), and integrating the Reynolds equations twice, the expression for pressure distribution is obtained as follows

$$\begin{aligned} p_{in} &= \frac{3\mu_{in}}{h_{in}^3} \left(Z_{in}^2 - \frac{1}{4}L_{in}^2 \right) \{ [(\omega + \omega_r)x_i - 2\dot{y}_i] \sin \alpha - [(\omega + \omega_r)y_i + 2\dot{x}_i] \cos \alpha \} \\ p_{out} &= \frac{3\mu_{out}}{h_{out}^3} \left(Z_{out}^2 - \frac{1}{4}L_{out}^2 \right) [(\omega_r X_r - 2\dot{Y}_r) \sin \beta - (\omega_r Y_r + 2\dot{X}_r) \cos \beta] \end{aligned} \tag{22}$$

The boundary conditions of inner and outer oil films are given as

$$\begin{aligned} p_{in}(\alpha_0) &= 0, \quad \left. \frac{\partial p_{in}}{\partial \alpha} \right|_{\alpha=\alpha_0} > 0 \\ p_{out}(\beta_0) &= 0, \quad \left. \frac{\partial p_{out}}{\partial \beta} \right|_{\beta=\beta_0} > 0 \end{aligned} \tag{23}$$

Based on Eq. (22) and Eq. (23), one has

$$\begin{aligned} \alpha_0 &= \arctan \frac{(\omega + \omega_r)y_i + 2\dot{x}_i}{(\omega + \omega_r)x_i - 2\dot{y}_i} \\ \beta_0 &= \arctan \frac{\omega_r Y_r + 2\dot{X}_r}{\omega_r X_r - 2\dot{Y}_r} \end{aligned} \tag{24}$$

Thus, the oil force of the inner oil film is

$$\begin{aligned}
 \begin{Bmatrix} F_{x,i}^{in} \\ F_{y,i}^{in} \end{Bmatrix} &= \int_{\alpha_0}^{\pi+\alpha_0} \int_{-\frac{1}{2}L_{in}}^{\frac{1}{2}L_{in}} p_{in} R_i \begin{Bmatrix} \cos \alpha \\ \sin \alpha \end{Bmatrix} dZ_{in} d\alpha \\
 &= -\frac{1}{2} \mu_{in} R_i L_{in}^3 A_i \int_{\alpha_0}^{\pi+\alpha_0} \frac{\cos \alpha_0 \sin \alpha - \sin \alpha_0 \cos \alpha}{h_{in}^3} \begin{Bmatrix} \cos \alpha \\ \sin \alpha \end{Bmatrix} d\alpha \quad (25) \\
 &= -\frac{1}{4} \mu_{in} R_i L_{in}^3 A_i \left(\cos \alpha_0 \begin{Bmatrix} \frac{\partial^2 G_1}{\partial x_i \partial y_i} \\ \frac{\partial^2 G_1}{\partial y_i^2} \end{Bmatrix} - \sin \alpha_0 \begin{Bmatrix} \frac{\partial^2 G_1}{\partial x_i^2} \\ \frac{\partial^2 G_1}{\partial x_i \partial y_i} \end{Bmatrix} \right)
 \end{aligned}$$

where

$$A_i = \sqrt{((\omega + \omega_r)x_i - 2\dot{y}_i)^2 + ((\omega + \omega_r)y_i + 2\dot{x}_i)^2} \quad (26)$$

$$G_1 = \int_{\alpha_0}^{\pi+\alpha_0} \frac{1}{h_{in}} d\alpha = \frac{2}{\sqrt{C_{in}^2 - x_i^2 - y_i^2}} \left[\frac{\pi}{2} + \arctan \left(\frac{y_i \cos \alpha_0 - x_i \sin \alpha_0}{\sqrt{C_{in}^2 - x_i^2 - y_i^2}} \right) \right] \quad (27)$$

From Eq. (27), yields

$$\frac{\partial^2 G_1}{\partial x_i^2} = \frac{G_1}{N_{i,1}} + \frac{3x_i^2 G_1}{N_{i,1}^2} + \frac{2N_{i,5}}{N_{i,1}N_{i,4}} + \frac{6x_i^2 N_{i,2}}{N_{i,1}^2 N_{i,4}} - \frac{2N_{i,3} \sin 2\alpha_0}{N_{i,4}^2} + \frac{4x_i N_{i,2} N_{i,3} \cos \alpha_0}{N_{i,1} N_{i,4}^2} \quad (28)$$

$$\frac{\partial^2 G_1}{\partial x_i \partial y_i} = \frac{3x_i y_i G_1}{N_{i,1}^2} + \frac{4x_i \cos \alpha_0}{N_{i,1} N_{i,4}} + \frac{6x_i y_i N_{i,2}}{N_{i,1}^2 N_{i,4}} - \frac{4N_{i,3} \sin^2 \alpha_0}{N_{i,4}^2} + \frac{4x_i N_{i,2} N_{i,3} \sin \alpha_0}{N_{i,1} N_{i,4}^2} \quad (29)$$

$$\frac{\partial^2 G_1}{\partial y_i^2} = \frac{G_1}{N_{i,1}} + \frac{3y_i^2 G_1}{N_{i,1}^2} + \frac{2N_{i,6}}{N_{i,1}N_{i,4}} + \frac{6y_i^2 N_{i,2}}{N_{i,1}^2 N_{i,4}} + \frac{2N_{i,3} \sin 2\alpha_0}{N_{i,4}^2} + \frac{4y_i N_{i,2} N_{i,3} \sin \alpha_0}{N_{i,1} N_{i,4}^2} \quad (30)$$

where $N_{i,1} = C_{in}^2 - x_i^2 - y_i^2$, $N_{i,2} = y_i \cos \alpha_0 - x_i \sin \alpha_0$, $N_{i,3} = x_i \cos \alpha_0 + y_i \sin \alpha_0$, $N_{i,4} = N_{i,1} + N_{i,2}^2$, $N_{i,5} = y_i \cos \alpha_0 - 3x_i \sin \alpha_0$, $N_{i,6} = 3y_i \cos \alpha_0 - x_i \sin \alpha_0$.

The oil force of the outer oil film is

$$\begin{aligned}
 \begin{Bmatrix} F_{x,i}^{out} \\ F_{y,i}^{out} \end{Bmatrix} &= \int_{\beta_0}^{\pi+\beta_0} \int_{-\frac{1}{2}L_{out}}^{\frac{1}{2}L_{out}} P_{out} R_r \begin{Bmatrix} \cos \beta \\ \sin \beta \end{Bmatrix} dZ_{out} d\beta \\
 &= -\frac{1}{2} \mu_{out} R_r L_{out}^3 A_r \int_{\beta_0}^{\pi+\beta_0} \frac{\cos \beta_0 \sin \beta - \sin \beta_0 \cos \beta}{h_{out}^3} \begin{Bmatrix} \cos \beta \\ \sin \beta \end{Bmatrix} d\beta \\
 &= -\frac{1}{4} \mu_{out} R_r L_{out}^3 A_r \left(\cos \beta_0 \begin{Bmatrix} \frac{\partial^2 G_2}{\partial X_r \partial Y_r} \\ \frac{\partial^2 G_2}{\partial Y_r^2} \end{Bmatrix} - \sin \beta_0 \begin{Bmatrix} \frac{\partial^2 G_2}{\partial X_r^2} \\ \frac{\partial^2 G_2}{\partial X_r \partial Y_r} \end{Bmatrix} \right)
 \end{aligned} \tag{31}$$

where

$$A_r = \sqrt{(\omega_r X_r - 2\dot{Y}_r)^2 + (\omega_r Y_r + 2\dot{X}_r)^2} \tag{32}$$

$$G_2 = \int_{\beta_0}^{\pi+\beta_0} \frac{1}{h_{out}} d\beta = \frac{2}{\sqrt{C_{out}^2 - X_r^2 - Y_r^2}} \left[\frac{\pi}{2} + \arctan \left(\frac{Y_r \cos \beta_0 - X_r \sin \beta_0}{\sqrt{C_{out}^2 - X_r^2 - Y_r^2}} \right) \right] \tag{33}$$

From Eq. (33), yields

$$\frac{\partial^2 G_2}{\partial X_r^2} = \frac{G_2}{N_{r,1}} + \frac{3X_r^2 G_2}{N_{r,1}^2} + \frac{2N_{r,5}}{N_{r,1} N_{r,4}} + \frac{6X_r^2 N_{r,2}}{N_{r,1}^2 N_{r,4}} - \frac{2N_{r,3} \sin 2\beta_0}{N_{r,4}^2} + \frac{4X_r N_{r,2} N_{r,3} \cos \beta_0}{N_{r,1} N_{r,4}^2} \tag{34}$$

$$\frac{\partial^2 G_2}{\partial X_r \partial Y_r} = \frac{3X_r Y_r G_2}{N_{r,1}^2} + \frac{4X_r \cos \beta_0}{N_{r,1} N_{r,4}} + \frac{6X_r Y_r N_{r,2}}{N_{r,1}^2 N_{r,4}} - \frac{4N_{r,3} \sin^2 \beta_0}{N_{r,4}^2} + \frac{4X_r N_{r,2} N_{r,3} \sin \beta_0}{N_{r,1} N_{r,4}^2} \tag{35}$$

$$\frac{\partial^2 G_2}{\partial Y_r^2} = \frac{G_2}{N_{r,1}} + \frac{3Y_r^2 G_2}{N_{r,1}^2} + \frac{2N_{r,6}}{N_{r,1} N_{r,4}} + \frac{6Y_r^2 N_{r,2}}{N_{r,1}^2 N_{r,4}} + \frac{2N_{r,3} \sin 2\beta_0}{N_{r,4}^2} + \frac{4Y_r N_{r,2} N_{r,3} \sin \beta_0}{N_{r,1} N_{r,4}^2} \tag{36}$$

where $N_{r,1} = C_{out}^2 - X_r^2 - Y_r^2$, $N_{r,2} = Y_r \cos \beta_0 - X_r \sin \beta_0$, $N_{r,3} = X_r \cos \beta_0 + Y_r \sin \beta_0$, $N_{r,4} = N_{r,1} + N_{r,2}^2$, $N_{r,5} = Y_r \cos \beta_0 - 3X_r \sin \beta_0$, $N_{r,6} = 3Y_r \cos \beta_0 - X_r \sin \beta_0$.

The floating ring is subjected to both the inner oil force and the outer oil force. The first floating ring bearing is located on disk 2. The second floating ring bearing is located on disk 3. The equations of the motion for the two floating rings can be given as

$$\begin{aligned}
 m_r \ddot{X}_{r1} &= F_{x,2}^{out} - F_{x,2}^{in} \\
 m_r \ddot{Y}_{r1} &= F_{y,2}^{out} - F_{y,2}^{in} - m_r g \cos \theta
 \end{aligned} \tag{37}$$

$$\begin{aligned}
 m_r \ddot{X}_{r2} &= F_{x,3}^{out} - F_{x,3}^{in} \\
 m_r \ddot{Y}_{r2} &= F_{y,3}^{out} - F_{y,3}^{in} - m_r g \cos \theta
 \end{aligned} \tag{38}$$

where m_r is the mass of floating ring.

The floating ring rotational speed ω_r largely determines the steady-state and dynamic force response of a floating ring bearing. An overly simplified analysis based on the short-length bearing model and nearly centered operation predicts a ring speed ratio equal to [30]

$$\frac{\omega_r}{\omega} = \frac{1}{1 + \mu_{out} L_{out} R_r^3 C_{in} / (\mu_{in} L_{in} R_r^3 C_{out})} \tag{39}$$

2.3 Nonlinear Dynamics of Turbocharger Rotor System

The governing differential equation of turbocharger rotor Eqs. (1)–(16) and floating ring bearings Eqs. (37)–(38) are combined to form the equation of system for the turbocharger system. The combined equation in matrix form is shown as:

$$\mathbf{M}\ddot{\mathbf{q}} + \omega \mathbf{G}\dot{\mathbf{q}} + \mathbf{K}\mathbf{q} = -\mathbf{F}_{oil} + \mathbf{F}_{ub} + \mathbf{F}_g \tag{40}$$

where \mathbf{M} is the mass matrix, \mathbf{G} is the gyroscopic matrix and of the rotor-FRB system, \mathbf{K} is the stiffness matrix, \mathbf{F}_{oil} is the oil force vector of floating ring bearing, \mathbf{F}_{ub} is the unbalance force vector, \mathbf{F}_g is the gravitational force vector. The expression of these

matrices and vectors are: $\mathbf{q} = \{ X \ Y \ X_r \ Y_r \}^T$, $X = \{ X_1 \ \varphi_{y1} \ X_2 \ \varphi_{y2} \ X_3 \ \varphi_{y3} \ X_4 \ \varphi_{y4} \}$,

$Y = \{ Y_1 \ \varphi_{x1} \ Y_2 \ \varphi_{x2} \ Y_3 \ \varphi_{x3} \ Y_4 \ \varphi_{x4} \}$, $X_r = \{ X_{r1} \ X_{r2} \}$, $Y_r = \{ Y_{r1} \ Y_{r2} \}$,

$$\mathbf{M} = \begin{bmatrix} \mathbf{M}_x & \mathbf{0}_{8 \times 8} & \mathbf{0}_{8 \times 4} \\ \mathbf{0}_{8 \times 8} & \mathbf{M}_y & \mathbf{0}_{8 \times 4} \\ \mathbf{0}_{4 \times 8} & \mathbf{0}_{4 \times 8} & \mathbf{M}_r \end{bmatrix}, \quad \mathbf{G} = \begin{bmatrix} \mathbf{0}_{8 \times 8} & \mathbf{G}_x & \mathbf{0}_{8 \times 4} \\ \mathbf{G}_y & \mathbf{0}_{8 \times 8} & \mathbf{0}_{8 \times 4} \\ \mathbf{0}_{4 \times 8} & \mathbf{0}_{4 \times 8} & \mathbf{0}_{4 \times 4} \end{bmatrix}, \quad \mathbf{K} = \begin{bmatrix} \mathbf{K}_x & \mathbf{0}_{8 \times 8} & \mathbf{0}_{8 \times 4} \\ \mathbf{0}_{8 \times 8} & \mathbf{K}_y & \mathbf{0}_{8 \times 4} \\ \mathbf{0}_{4 \times 8} & \mathbf{0}_{4 \times 8} & \mathbf{0}_{4 \times 4} \end{bmatrix},$$

$$\mathbf{M}_x = \mathbf{M}_y = \text{diag} \{ m_1 \ J_{a1} \ m_2 \ J_{a2} \ m_3 \ J_{a3} \ m_4 \ J_{a4} \}, \quad \mathbf{M}_r = \text{diag} \{ m_r \ m_r \ m_r \ m_r \},$$

$$\mathbf{G}_x = -\mathbf{G}_y = \text{diag} \{ 0 \ -J_{p1} \ 0 \ -J_{p2} \ 0 \ -J_{p3} \ 0 \ -J_{p4} \}, \quad \mathbf{K}_x = \begin{bmatrix} \mathbf{K}_{x11} & \mathbf{K}_{x12} \\ \mathbf{K}_{x21} & \mathbf{K}_{x22} \end{bmatrix},$$

$$\mathbf{K}_{x11} = \begin{bmatrix} \frac{12EI_1}{l_1^3} & \frac{6EI_1}{l_1^2} & -\frac{12EI_1}{l_1^3} & \frac{6EI_1}{l_1^2} \\ \frac{6EI_1}{l_1^2} & \frac{4EI_1}{l_1} & -\frac{6EI_1}{l_1^2} & \frac{2EI_1}{l_1} \\ -\frac{12EI_1}{l_1^2} & -\frac{6EI_1}{l_1} & \frac{12EI_1}{l_1^2} + \frac{12EI_2}{l_2^2} & -\frac{6EI_1}{l_1} + \frac{6EI_2}{l_2} \\ \frac{6EI_1}{l_1^2} & \frac{2EI_1}{l_1} & -\frac{6EI_1}{l_1^2} + \frac{6EI_2}{l_2^2} & \frac{4EI_1}{l_1} + \frac{4EI_2}{l_2} \end{bmatrix}, \quad \mathbf{K}_{x12} = \begin{bmatrix} 0 & 0 & 0 & 0 \\ 0 & 0 & 0 & 0 \\ -\frac{12EI_2}{l_2^2} & \frac{6EI_2}{l_2} & 0 & 0 \\ -\frac{6EI_2}{l_2^2} & \frac{2EI_2}{l_2} & 0 & 0 \end{bmatrix},$$

$$\mathbf{K}_{x21} = \begin{bmatrix} 0 & 0 & -\frac{12EI_2}{l_2^2} & -\frac{6EI_2}{l_2} \\ 0 & 0 & \frac{6EI_2}{l_2} & \frac{2EI_2}{l_2} \\ 0 & 0 & 0 & 0 \\ 0 & 0 & 0 & 0 \end{bmatrix}, \quad \mathbf{K}_{x22} = \begin{bmatrix} \frac{12EI_2}{l_2^2} + \frac{12EI_3}{l_3^2} & -\frac{6EI_2}{l_2} + \frac{6EI_3}{l_3} & -\frac{12EI_3}{l_3^2} & \frac{6EI_3}{l_3} \\ -\frac{6EI_2}{l_2} + \frac{6EI_3}{l_3} & \frac{4EI_2}{l_2} + \frac{4EI_3}{l_3} & -\frac{6EI_3}{l_3^2} & \frac{2EI_3}{l_3} \\ -\frac{12EI_3}{l_3^2} & -\frac{6EI_3}{l_3} & \frac{12EI_3}{l_3^2} & -\frac{6EI_3}{l_3} \\ \frac{6EI_3}{l_3^2} & \frac{2EI_3}{l_3} & -\frac{6EI_3}{l_3^2} & \frac{4EI_3}{l_3} \end{bmatrix},$$

$$\mathbf{K}_y = \begin{bmatrix} \mathbf{K}_{y11} & \mathbf{K}_{y12} \\ \mathbf{K}_{y21} & \mathbf{K}_{y22} \end{bmatrix}, \quad \mathbf{K}_{y11} = \begin{bmatrix} \frac{12EI_1}{l_1^3} & -\frac{6EI_1}{l_1^2} & -\frac{12EI_1}{l_1^3} & -\frac{6EI_1}{l_1^2} \\ -\frac{6EI_1}{l_1^2} & \frac{4EI_1}{l_1} & \frac{6EI_1}{l_1^2} & \frac{2EI_1}{l_1} \\ -\frac{12EI_1}{l_1^3} & \frac{6EI_1}{l_1^2} & \frac{12EI_1}{l_1^3} + \frac{12EI_2}{l_1^3} & \frac{6EI_1}{l_1^2} - \frac{6EI_2}{l_1^2} \\ -\frac{6EI_1}{l_1^2} & \frac{2EI_1}{l_1} & \frac{6EI_1}{l_1^2} - \frac{6EI_2}{l_1^2} & \frac{4EI_1}{l_1} + \frac{4EI_2}{l_1} \end{bmatrix},$$

$$\mathbf{K}_{y12} = \begin{bmatrix} 0 & 0 & 0 & 0 \\ 0 & 0 & 0 & 0 \\ -\frac{12EI_2}{l_2^3} & -\frac{6EI_2}{l_2^2} & 0 & 0 \\ \frac{6EI_2}{l_2^2} & \frac{2EI_2}{l_2} & 0 & 0 \end{bmatrix}, \quad \mathbf{K}_{y21} = \begin{bmatrix} 0 & 0 & -\frac{12EI_2}{l_2^3} & \frac{6EI_2}{l_2^2} \\ 0 & 0 & -\frac{6EI_2}{l_2^2} & \frac{2EI_2}{l_2} \\ 0 & 0 & 0 & 0 \\ 0 & 0 & 0 & 0 \end{bmatrix},$$

$$\mathbf{K}_{y22} = \begin{bmatrix} \frac{12EI_2}{l_2^3} + \frac{12EI_3}{l_2^3} & \frac{6EI_2}{l_2^2} - \frac{6EI_3}{l_2^2} & -\frac{12EI_3}{l_2^3} & -\frac{6EI_3}{l_2^2} \\ \frac{6EI_2}{l_2^2} - \frac{6EI_3}{l_2^2} & \frac{4EI_2}{l_2} + \frac{4EI_3}{l_2} & \frac{6EI_3}{l_2^2} & \frac{2EI_3}{l_2} \\ -\frac{12EI_3}{l_2^3} & \frac{6EI_3}{l_2^2} & \frac{12EI_3}{l_2^3} & \frac{6EI_3}{l_2^2} \\ -\frac{6EI_3}{l_2^2} & \frac{2EI_3}{l_2} & \frac{6EI_3}{l_2^2} & \frac{4EI_3}{l_2} \end{bmatrix}, \quad \mathbf{F}_{oil} = \{ \mathbf{F}_{o,x} \ \mathbf{F}_{o,y} \ \mathbf{F}_{o,r} \}^T,$$

$$\mathbf{F}_{o,x} = \{ 0 \ 0 \ F_{x,2}^{in} \ 0 \ F_{x,3}^{in} \ 0 \ 0 \ 0 \}, \quad \mathbf{F}_{o,y} = \{ 0 \ 0 \ F_{y,2}^{in} \ 0 \ F_{y,3}^{in} \ 0 \ 0 \ 0 \},$$

$$\mathbf{F}_{o,r} = \{ F_{x,2}^{out} - F_{x,2}^{in} \ F_{x,3}^{out} - F_{x,3}^{in} \ F_{y,2}^{out} - F_{y,2}^{in} \ F_{y,3}^{out} - F_{y,3}^{in} \}, \quad \mathbf{F}_{ub} = \{ \mathbf{F}_{ub,x} \ \mathbf{F}_{ub,y} \ \mathbf{F}_{ub,r} \}^T,$$

$$\mathbf{F}_{ub,x} = \{ m_1 e_1 \omega^2 \cos \omega t \ 0 \ 0 \ 0 \ 0 \ 0 \ m_4 e_4 \omega^2 \cos \omega t \ 0 \}, \quad \mathbf{F}_{ub,y} = \{ m_1 e_1 \omega^2 \sin \omega t \ 0 \ 0 \ 0 \ 0 \ 0 \ m_4 e_4 \omega^2 \sin \omega t \ 0 \},$$

$$\mathbf{F}_{ub,r} = \mathbf{0}_{1 \times 4}, \quad \mathbf{F}_g = \{ \mathbf{F}_{g,x} \ \mathbf{F}_{g,y} \ \mathbf{F}_{g,r} \}^T, \quad \mathbf{F}_{g,x} = \mathbf{0}_{1 \times 8},$$

$$\mathbf{F}_{g,y} = \{ -m_1 g \cos \theta \ 0 \ -m_2 g \cos \theta \ 0 \ -m_3 g \cos \theta \ 0 \ -m_4 g \cos \theta \ 0 \}, \quad \mathbf{F}_{g,r} = \{ 0 \ 0 \ -m_r g \cos \theta \ -m_r g \cos \theta \}.$$

3 The Critical Speed of Nonlinear Turbocharger Rotor System

From Eq. (40), the static displacement of the turbocharger rotor system due to gravity can be obtained by solving the following equation.

$$Kq_0 = -F_{oil}(q_0) + F_g \tag{41}$$

where F_{oil} is a nonlinear function for q_0 , and q_0 is the static balance position.

Substituting $q = \bar{q}(t) + q_0$ into Eq. (40), yields

$$M\ddot{\bar{q}} + \omega G\dot{\bar{q}} + K\bar{q} + Kq_0 = -F_{oil} + F_{ub} + F_g \tag{42}$$

The Taylor expansion of nonlinear oil force F_{oil} in q_0 is

$$F_{oil} = F_{oil}(q_0) + K_{oil}\bar{q} + N_2(\bar{q}^2) + N_3(\bar{q}^3) + \dots \tag{43}$$

where

$$K_{oil} = \frac{\partial F_{oil}(q_0)}{\partial q} \tag{44}$$

Substituting Eq. (41) and Eq. (43) into Eq. (42) and neglecting the nonlinear terms, one has

$$M\ddot{\bar{q}} + \omega G\dot{\bar{q}} + (K + K_{oil})\bar{q} = F_{ub} \quad (45)$$

The solution of Eq. (45) is

$$\bar{q} = ue^{\lambda t} \quad (46)$$

The frequency of the turbocharger rotor system can be obtained by solving the following eigenvalue problem.

$$(\lambda^2 \mathbf{M} + \lambda \omega \mathbf{G} + \mathbf{K} + \mathbf{K}_{oil})\mathbf{u} = \mathbf{0} \quad (47)$$

One can also solve the following generalized eigenvalue problem.

$$(\lambda \mathbf{P} + \mathbf{Q}) \begin{Bmatrix} \mathbf{u} \\ \lambda \mathbf{u} \end{Bmatrix} = \mathbf{0} \quad (48)$$

where

$$\mathbf{P} = \begin{bmatrix} \omega \mathbf{G} & \mathbf{M} \\ \mathbf{M} & \mathbf{0} \end{bmatrix} \quad (49)$$

$$\mathbf{Q} = \begin{bmatrix} \mathbf{K} + \mathbf{K}_{oil} & \mathbf{0} \\ \mathbf{0} & -\mathbf{M} \end{bmatrix} \quad (50)$$

The eigenvalues of Eq. (48) are image, i.e., $\lambda = i\omega_n$. The positive ω_n means a forward mode (precession motions in the same sense of rotation as the own rotation of the shaft) and the negative ω_n means a backward mode. The evolution of ω_n as a function of the rotational speed of the rotor gives a Campbell diagram in the rotating frame. The critical speeds of the turbocharger rotor system are the intersection of the line $\omega_n = \omega$ and the different order frequency curves in the Campbell diagram.

4 Results and Discussions

The turbocharger rotor-floating ring bearing system is a highly nonlinear system. However, the linear behavior of the system is still important to understand the nonlinear responses of this system. In this section, the critical speed of an inclined turbocharger rotor system is investigated. The main parameters are given in Table 1.

From Eq. (41), the static balance position \mathbf{q}_0 is determined by the gravitational force vector. It means \mathbf{q}_0 is affected by the inclined angle θ . Moreover, \mathbf{K}_{oil} is determined by \mathbf{q}_0 . From Eq. (47), we can conclude that the natural frequency of the linear system of turbocharger rotor system is affected by θ . The natural frequencies of the linear system of turbocharger rotor system under five inclined angle θ , i.e. 0° , 30° , 45° , 60° , and 90° , are studied in the following.

Table 1 Parameters of the rotor and floating ring

Parameter	Value
Mass of disk	$m_1 = 0.7787$ kg, $m_2 = 0.0935$ kg $m_3 = 0.0891$ kg, $m_4 = 1.5591$ kg
Mass of floating ring	$m_r = 0.055$ kg
Polar moment of inertia	$J_{p1} = 6.72 \times 10^{-4}$ kg·m ² , $J_{p2} = 4.98 \times 10^{-6}$ kg·m ² $J_{p3} = 4.50 \times 10^{-6}$ kg·m ² , $J_{p4} = 1.426 \times 10^{-3}$ kg·m ²
Transverse moment of inertia	$J_{a1} = 4.61 \times 10^{-4}$ kg·m ² , $J_{a2} = 62.46 \times 10^{-6}$ kg·m ² $J_{a3} = 62.22 \times 10^{-6}$ kg·m ² , $J_{a4} = 5.5 \times 10^{-3}$ kg·m ²
Young's modulus	$E = 212$ Gpa
Length of rotor section	$l_1 = 27.0$ mm, $l_2 = 58.0$ mm, $l_3 = 22.0$ mm
Diameter of rotor section	$d_1 = 12.7$ mm, $d_2 = 17.4$ mm, $d_3 = 17.4$ mm
Moment of inertia of rotor section	$I_1 = 2.3527 \times 10^{-9}$ m ⁴ , $I_2 = I_3 = 4.4995 \times 10^{-9}$ m ⁴
Radius of journal	$R_j = 8.696$ mm
Outer radius of the floating ring	$R_r = 13.9475$ mm
Viscosity of oil film	$\mu_{in} = \mu_{out} = 12.77 \times 10^{-3}$ pa·s
Length of oil film	$L_{in} = 14.0$ mm, $L_{out} = 17.0$ mm
Radial clearance of oil film	$C_{in} = 0.034$ mm, $C_{out} = 0.057$ mm

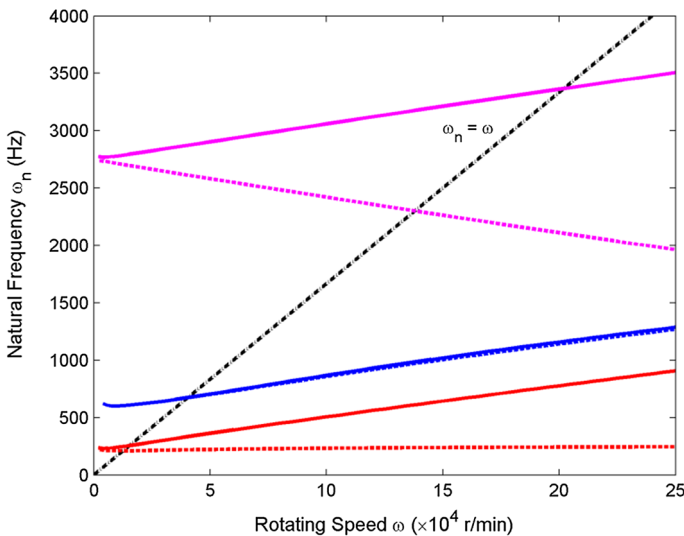


Fig. 3 The Campbell diagram of turbocharger rotor system with $\theta = 0^\circ$

When $\theta = 0^\circ$, the Campbell diagram of the turbocharger rotor system is shown in Fig. 3. The forward mode is indicated by solid line, while the backward mode is marked by dash line. The dash-dot line means $\omega_n = \omega$. The intersection of dash-dot line and solid line is the critical speed of forward mode. The intersection of dash-dot line and dash line is the critical speed of backward mode.

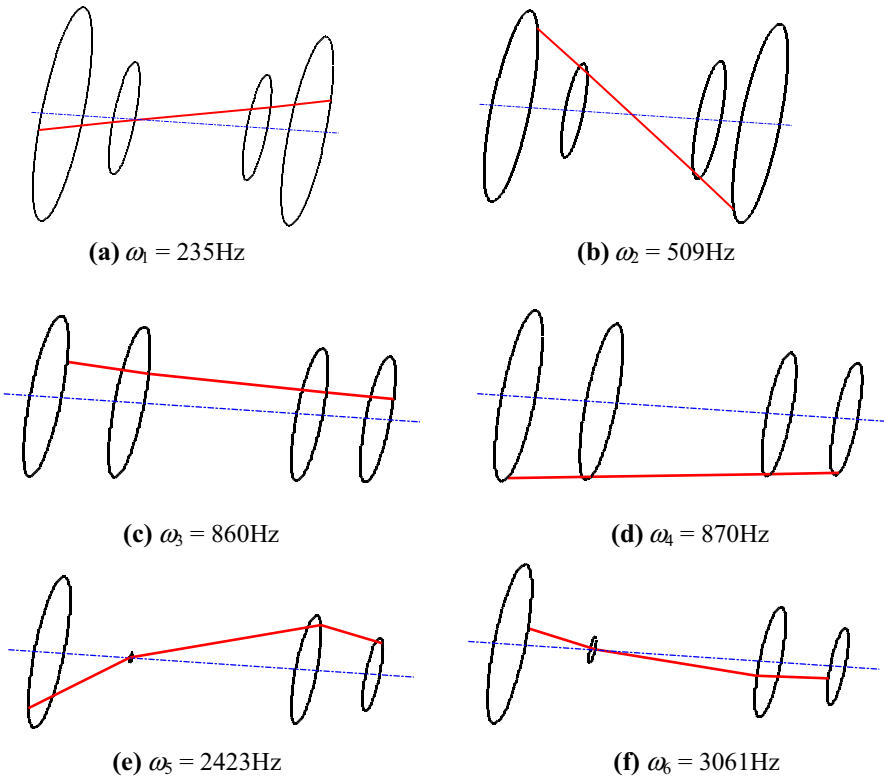


Fig. 4 Mode shapes of turbocharger rotor system with $\omega = 100,000$ r/min and $\theta = 0^\circ$

In order to reveal the mode shape of the turbocharger rotor system, the first six rotor mode shapes when the rotating speed is 100000 r/min are given in Fig. 4. What can be appreciated is that the first four modes are rigid modes, the fifth and sixth modes are bending modes. The first mode is a conical whirl backward mode. The second mode is a conical whirl forward mode. The third mode is a cylindrical whirl backward mode. The fourth mode is a cylindrical whirl forward mode. The fifth mode is a bending backward mode. The sixth mode is a bending forward mode.

From Fig. 3, we can see that the critical speed of the conical whirl backward mode is 12768 r/min. The critical speed of the conical whirl forward mode is 15497 r/min. The critical speed of the cylindrical whirl backward mode is 40504 r/min. The critical speed of the cylindrical whirl forward mode is 40594 r/min. The critical speed of the bending backward mode is 138142 r/min. The critical speed of the bending forward mode is 202203 r/min.

The Campbell diagram of the turbocharger rotor system when the inclined angle θ is 30° is presented in Fig. 5. It shows that the critical speeds of all the modes are decreased. The critical speed of the conical whirl backward mode is 11959 r/min. The critical speed of the conical whirl forward mode is 14535 r/min.

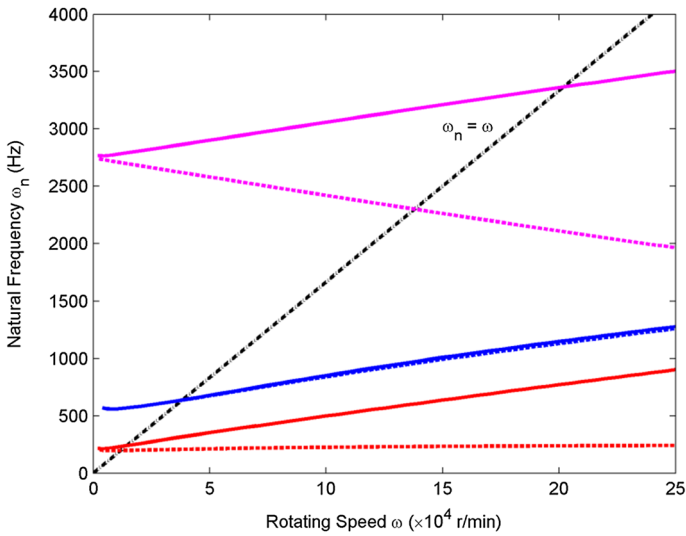


Fig. 5 The Campbell diagram of turbocharger rotor system with $\theta=30^\circ$

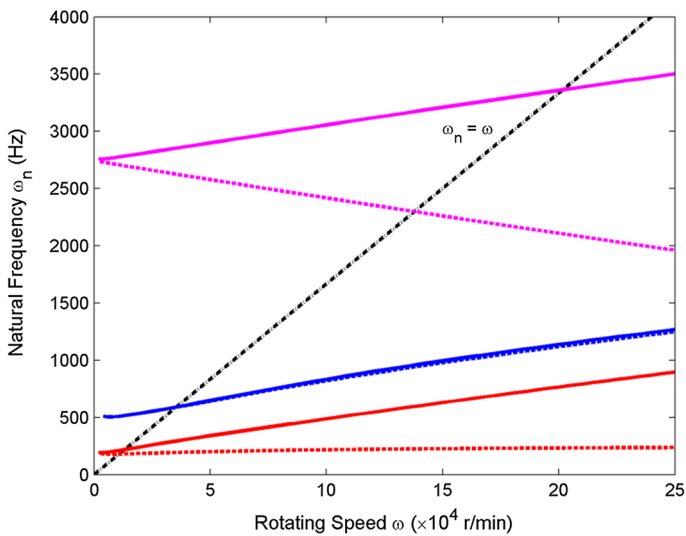


Fig. 6 The Campbell diagram of turbocharger rotor system with $\theta=45^\circ$

The critical speed of the cylindrical whirl backward mode is 38310 r/min. The critical speed of the cylindrical whirl forward mode is 38419 r/min. The critical speed of the bending backward mode is 138076 r/min. The critical speed of the bending forward mode is 202089 r/min.

When the inclined angle θ is increased to 45° the Campbell diagram of the turbocharger rotor system is plotted in Fig. 6. The critical speeds of all the modes

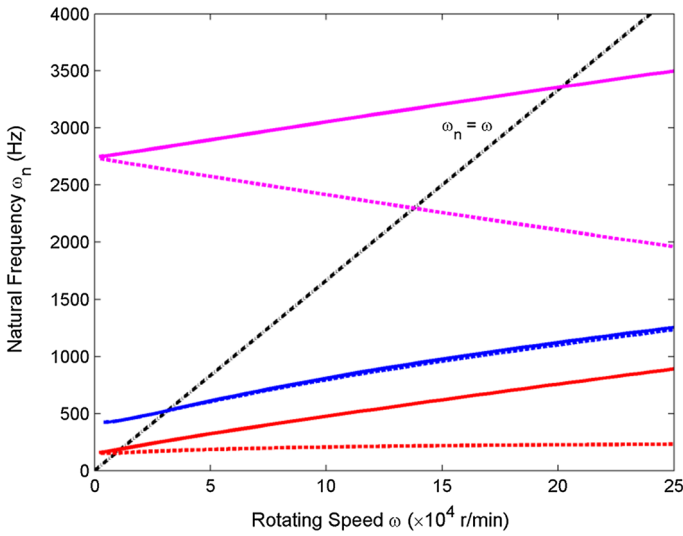


Fig. 7 The Campbell diagram of turbocharger rotor system with $\theta=60^\circ$

are further decreased. The critical speed of the conical whirl backward mode is 10915 r/min. The critical speed of the conical whirl forward mode is 13306 r/min. The critical speed of the cylindrical whirl backward mode is 35527 r/min. The critical speed of the cylindrical whirl forward mode is 35664 r/min. The critical speed of the bending backward mode is 137997 r/min. The critical speed of the bending forward mode is 201953 r/min.

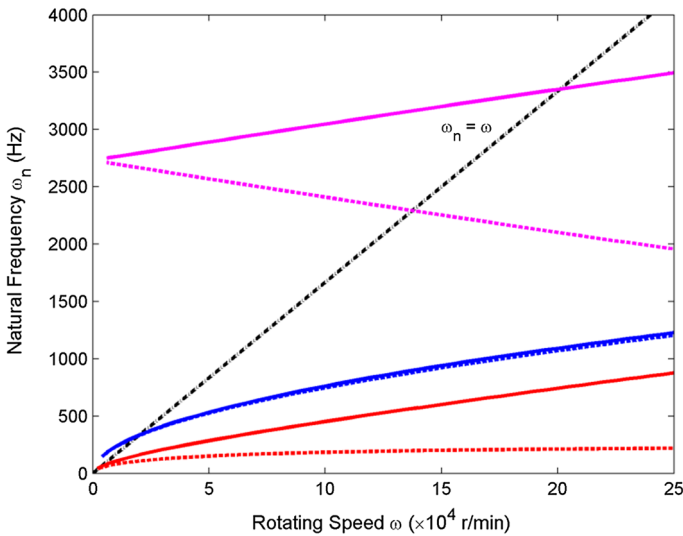


Fig. 8 The Campbell diagram of turbocharger rotor system with $\theta=90^\circ$

Table 2 The critical speed of turbocharger rotor system with different inclined angle

θ	Critical speed (r/min)					
	Conical whirl		Cylindrical whirl		Bending	
	Backward	Forward	Backward	Forward	Backward	Forward
0°	12,768	15,497	40,504	40,594	138,142	202,203
30°	11,959	14,535	38,310	38,419	138,076	202,089
45°	10,915	13,306	35,527	35,664	137,997	201,953
60°	9374	11,481	31,553	31,740	137,893	201,777
90°	2724	3863	20,047	20,408	137,640	201,355

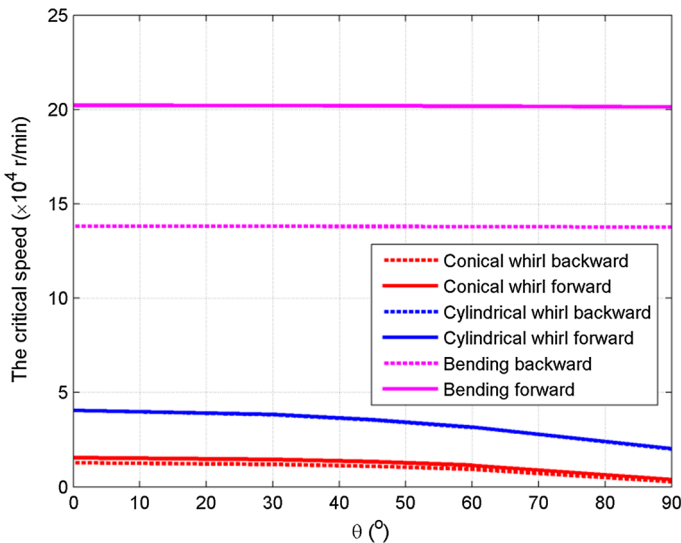


Fig. 9 The critical speed of turbocharger rotor system with different inclined angle

When the inclined angle θ is increased to 60° the Campbell diagram of the turbocharger rotor system is given in Fig. 7. The critical speeds of all the modes are also decreased. The critical speed of the conical whirl backward mode is 9374 r/min. The critical speed of the conical whirl forward mode is 11481 r/min. The critical speed of the cylindrical whirl backward mode is 31553 r/min. The critical speed of the cylindrical whirl forward mode is 31740 r/min. The critical speed of the bending backward mode is 137893 r/min. The critical speed of the bending forward mode is 201777 r/min.

When the turbocharger rotor is vertical, i.e. $\theta=90^\circ$, the Campbell diagram of the turbocharger rotor system is revealed in Fig. 8. The critical speeds of all the modes are decreased greatly. The critical speed of the conical whirl backward mode is 2724 r/min. The critical speed of the conical whirl forward mode is 3863 r/min. The critical speed of the cylindrical whirl backward mode is 20047 r/min. The critical

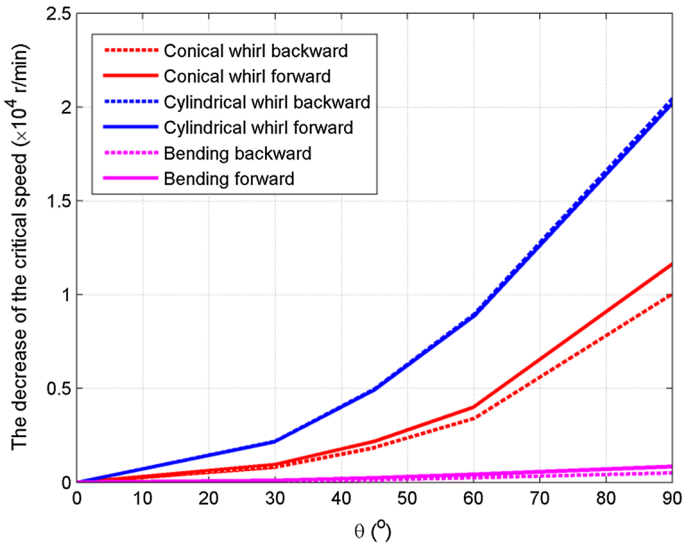


Fig. 10 The decrease of critical speed of turbocharger rotor system with different inclined angle

speed of the cylindrical whirl forward mode is 20408 r/min. The critical speed of the bending backward mode is 137640 r/min. The critical speed of the bending forward mode is 201355 r/min.

Table 2 and Fig. 9 show the critical speed of the turbocharger rotor system under different inclined angle θ . It clearly shows that the critical speed of the turbocharger rotor system is decreased as the inclined angle θ increases.

Figure 10 depicts the decrease of the critical speed versus inclined angle. One can see that the critical speed decreases of backward and forward with the same vibration mode are almost the same. Moreover, among the three vibration modes, i.e. conical whirl, cylindrical whirl, and bending, the critical speed of cylindrical whirl furnishes the highest decrease while the critical speed of bending attains the lowest decrease. In order to avoid resonance, the rotating speed of the turbocharger rotor should be far from the critical speed. Actually, the turbocharger rotor is operating in a quite wide speed range which is between the critical speed of cylindrical whirl mode and the critical speed of bending mode. More important the operating speed range is enlarged when the inclined angle of the turbocharger rotor is increased from 0 to 90°. It means the vertical turbocharger rotor has a more wide operating speed range than the horizontal turbocharger rotor.

5 Conclusions

In order to reveal the influence of weight on the critical speed of an inclined turbocharger rotor coupled with floating ring bearings, the nonlinear dynamic model of the turbocharger rotor system is derived using the lumped mass model and the

Capone's model. The critical speed of the linear system of the turbocharger rotor system is calculated. Three vibration modes, i.e. conical whirl, cylindrical whirl, and bending are obtained. Increasing the inclined angle would decrease the critical speed. Among the three vibration modes, the critical speed of cylindrical whirl furnishes the highest decrease while the critical speed of bending attains the lowest decrease. The vertical turbocharger rotor has a more wide operating speed range than the horizontal turbocharger rotor.

Acknowledgements The author is indebted to the reviewers for helpful suggestions and insights concerning the presentation of this paper.

Author contributions XO constructed the dynamic model. HG participated the modeling and drafted the manuscript. XW participated in the modeling and coordination of the study. RM and ML carried out the calculation. SC improved the manuscript. All authors read and approved the final manuscript.

Funding This work is supported by the National Natural Science Foundation of China (Grant Nos. 12172247, 12021002).

Availability of data and material All data used to support the findings of this study are available from the corresponding author upon request.

Declarations

Conflict of interest The authors declare that there is no conflict of interest regarding the publication of this paper.

Open Access This article is licensed under a Creative Commons Attribution 4.0 International License, which permits use, sharing, adaptation, distribution and reproduction in any medium or format, as long as you give appropriate credit to the original author(s) and the source, provide a link to the Creative Commons licence, and indicate if changes were made. The images or other third party material in this article are included in the article's Creative Commons licence, unless indicated otherwise in a credit line to the material. If material is not included in the article's Creative Commons licence and your intended use is not permitted by statutory regulation or exceeds the permitted use, you will need to obtain permission directly from the copyright holder. To view a copy of this licence, visit <http://creativecommons.org/licenses/by/4.0/>.

References

1. Pettinato, B.C., DeChoudhury, P.: Rotordynamic and bearing upgrade of a high-speed turbocharger. *J. Eng. Gas Turb. Power* **125**, 95–101 (2003)
2. Chen, W.J.: Rotordynamics and bearing design of turbochargers. *Mech. Syst. Signal. Pr.* **29**, 77–89 (2012)
3. Ying, G.C., Meng, G., Jing, J.P.: Turbocharger rotor dynamics with foundation excitation. *Arch. Appl. Mech.* **79**, 287–299 (2009)
4. Andres, L.S., Rivadeneira, J.C., Gjika, K., et al.: Rotordynamics of small turbochargers supported on floating ring bearings—highlights in bearing analysis and experimental validation. *J. Tribol. T. ASME* **129**, 391–397 (2007)
5. San Andres, L., Rivadeneira, J.C., Chinta, M., et al.: Nonlinear rotordynamics of automotive turbochargers: predictions and comparisons to test data. *J. Eng. Gas Turb. Power* **129**, 488–493 (2007)
6. Schweizer, B.: Dynamics and stability of turbocharger rotors. *Arch. Appl. Mech.* **80**, 1017–1043 (2010)

7. Lu, K., Jin, Y., Chen, Y., et al.: Review for order reduction based on proper orthogonal decomposition and outlooks of applications in mechanical systems. *Mech. Syst. Signal. Pr.* **123**, 264–297 (2019)
8. Hou, L., Chen, Y., Fu, Y., et al.: Application of the HB-AFT method to the primary resonance analysis of a dual-rotor system. *Nonlinear Dyn.* **88**, 2531–2551 (2017)
9. He, D., Yang, Y., Xu, H., et al.: Dynamic analysis of rolling bearings with roller spalling defects based on explicit finite element method and experiment. *J. Nonlinear Math. Phys.* (2022). <https://doi.org/10.1007/s44198-022-00027-y>
10. Kirk, R.G., Alsaeed, A.A., Gunter, E.J.: Stability analysis of a high-speed automotive turbocharger. *Tribol. T.* **50**, 427–434 (2007)
11. Schilder, F., Rubel, J., Starke, J., et al.: Efficient computation of quasiperiodic oscillations in nonlinear systems with fast rotating parts. *Nonlinear Dyn.* **51**, 529–539 (2008)
12. Schweizer, B.: Total instability of turbocharger rotors-physical explanation of the dynamic failure of rotors with full-floating ring bearings. *J. Sound Vib.* **328**, 156–190 (2009)
13. Schweizer, B.: Oil whirl, oil whip and whirl/whip synchronization occurring in rotor systems with full-floating ring bearings. *Nonlinear Dyn.* **57**, 509–532 (2009)
14. Bonello, P.: Transient modal analysis of the non-linear dynamics of a turbocharger on floating ring bearings. *P. I. Mech. Eng. J-J. Eng.* **223**, 79–93 (2009)
15. Tian, L., Wang, W.J., Peng, Z.J.: Dynamic behaviours of a full floating ring bearing supported turbocharger rotor with engine excitation. *J. Sound Vib.* **330**, 4851–4874 (2011)
16. Tian, L., Wang, W.J., Peng, Z.J.: Nonlinear effects of unbalance in the rotor-floating ring bearing system of turbochargers. *Mech. Syst. Signal. Pr.* **34**, 298–320 (2013)
17. Koutsovasilis, P., Driot, N., Lu, D.X.N., et al.: Quantification of sub-synchronous vibrations for turbocharger rotors with full-floating ring bearings. *Arch. Appl. Mech.* **85**, 481–502 (2015)
18. Liang, F., Zhou, M., Xu, Q.Y.: Effects of semi-floating ring bearing outer clearance on the sub-synchronous oscillation of turbocharger rotor. *Chin. J. Mech. Eng.-En.* **29**, 901–910 (2016)
19. Smolik, L., Hajzman, M., Byrtus, M.: Investigation of bearing clearance effects in dynamics of turbochargers. *Int. J. Mech. Sci.* **127**, 62–72 (2017)
20. Zhang, C.C., Men, R.X., He, H., et al.: Effects of circumferential and axial grooves on the nonlinear oscillations of the full floating ring bearing supported turbocharger rotor. *P. I. Mech. Eng. J-J. Eng.* **233**, 741–757 (2019)
21. Singh, A., Gupta, T.C.: Effect of rotating unbalance and engine excitations on the nonlinear dynamic response of turbocharger flexible rotor system supported on floating ring bearings. *Arch. Appl. Mech.* **90**, 1117–1134 (2020)
22. Shi, M.L., Wang, D.Z., Zhang, J.G.: Nonlinear dynamic analysis of a vertical rotor-bearing system. *J. Mech. Sci. Technol.* **27**, 9–19 (2013)
23. Luneno, J.C., Aidanpaa, J.O., Gustavsson, R.: Experimental verification of a combi-bearing model for vertical rotor systems. *J. Vib. Acoust.* (2013). <https://doi.org/10.1115/1.4023052>
24. Cha, M., Glavatskih, S.: Nonlinear dynamic behaviour of vertical and horizontal rotors in compliant liner tilting pad journal bearings: Some design considerations. *Tribol. Int.* **82**, 142–152 (2015)
25. Nishimura, A., Inoue, T., Watanabe, Y.: Nonlinear analysis and characteristic variation of self-excited vibration in the vertical rotor system due to the flexible support of the journal bearing. *J. Vib. Acoust.* (2018). <https://doi.org/10.1115/1.4037520>
26. Shi, Z.Y., Jin, Y.Z., Yuan, X.Y.: Influence of pivot design on nonlinear dynamic analysis of vertical and horizontal rotors in tilting pad journal bearings. *Tribol. Int.* (2019). <https://doi.org/10.1016/j.triboint.2019.105859>
27. Liu, Z.S., Qian, D.S., Sun, L.Q., et al.: Stability analyses of inclined rotor bearing system based on non-linear oil film force models. *P. I. Mech. Eng. C-J. Mec.* **226**, 439–453 (2012)
28. Qian, D.S., Liu, Z.S., Yan, J.J., et al.: Numerical and experimental research on periodic solution stability of inclined rotor journal bearing system. *Proc Asme Turbo Expo* **226**, 321–330 (2012)
29. Xu, X.P., Han, Q.K., Chu, F.L.: Dynamic responses and vibration characteristics for an inclined rotor with unbalanced magnetic excitation. *Proceedings of the Fourteenth International Federation for the Promotion of Mechanism and Machine Science World Congress 192–200* (2015).
30. Shaw, M.C., Nussdorfer, T.J.: An analysis of the full floating journal bearing. *NACA report*, (1947).